

Dynamic thermal rating of power lines – Model and measurements in rainy conditions



G. Kosec^a, M. Maksić^{b,*}, V. Djurica^b

^aJožef Stefan Institute, Jamova 39, 1000 Ljubljana, Slovenia

^bMilan Vidmar Electric Power Research Institute, Hajdrihova 2, Ljubljana, Slovenia

ARTICLE INFO

Article history:

Received 27 October 2016

Received in revised form 21 February 2017

Accepted 2 April 2017

Keywords:

Dynamic thermal rating

Transmission lines

Numerical model

Rain

Measurements

ABSTRACT

The transfer capabilities of overhead power lines are often limited by the critical power line temperature that depends on the magnitude of the transferred current and the ambient conditions, i.e. ambient temperature, wind, precipitation, etc. To utilize existing power lines more effectively and more safely concerning the critical power line temperatures and to enforce safety measures during potentially dangerous events, dynamic assessment of the thermal rating is required. In this paper, a Dynamic Thermal Rating model that covers the most important weather phenomena, with special emphasis on rain, is presented. The model considers a dynamic heat generation due to the Joule losses within the conductor and heat exchange with the surrounding in terms of convection, radiation, evaporation, rain impinging and solar heating. The model is validated by comparison of the skin and core temperature of the power line with measurements under realistic environmental conditions.

© 2017 Elsevier Ltd. All rights reserved.

1. Introduction

The increasing complexity of electrical power systems and increased demands for electrical power constantly pressure the transmission system operators (TSOs) to improve transmission capabilities. The placement of new transmission lines into the system, which is immediate solution to the problem, is unfortunately limited due to the difficulty of acquiring new transmission line corridors, the extensive financial burden and vast societal consensus for the environmental care. As a result, some existing lines are already overloaded causing bottlenecks that may and have already caused blackouts in the past [1]. The TSOs are thus striving to increase transmission capacity of existing overhead lines without compromising system stability.

The transmission capacity, i.e. maximum allowed current, is often limited by the maximum allowed temperature of the conductor. The temperature of the power line must not exceed a certain value, e.g. 80 °C in the Slovenian power system, which determines the maximal permissible sag of the power line. The temperature of the power line also affects the resistance and consequently the power loss [2], while its variation plays an important role in the structural decay of the power line [3]. Traditionally, the current

carrying capacity of the line is assessed for unfavourable weather conditions, namely ambient temperature of 35 °C and wind velocity of 0.6 m/s without rain [4]. A more sophisticated approach is to dynamically determine the capacity considering the current weather conditions or the weather forecast, which would result in an increase of the current carrying capacity of the line, since most of the time more favourable conditions are expected. However, in order to implement dynamic determination of maximal allowed current, the temperature of the overhead line at given conditions has to be known.

The most straightforward approach to determine the power line temperature would be direct measurement, e.g., with Overhead Transmission Line Monitoring system (OTLM) devices [5]. Such an approach would, however, require vast number of measuring devices to effectively cover the whole power system. An alternative is a class of emerging indirect estimates that rely on the measurements of line resistance using synchronous voltage and current measurements by phase measurement units (PMUs) [6–9]. This alternative requires installation of several PMUs and adequate state estimation algorithms. Another option, considered in this paper, is to model the heat generation and exchange between the line and the surroundings to compute the line temperature.

With an appropriate physical model, a TSO can use metrological measurements combined with the weather forecast to predict line temperature in all segments of the transmission line and hence identify potential hot spots, i.e. spans with expected critical

* Corresponding author.

E-mail addresses: gregor.kosec@ijs.si (G. Kosec), milos.maksic@eimv.si (M. Maksić), vladimir.djurica@eimv.si (V. Djurica).

temperature. Such Dynamic Thermal Rating (DTR) systems have been developed for the past 30 years [10]. The CIGRE [11] and IEEE [12] guidelines usually serve as base models for evaluating line temperatures and thermal currents of overhead lines based on ambient conditions. Various discussions on DTR systems and their practical application can be found in [11]. The DTR model parameter uncertainty, as well as the diversity of uncertainty sources, has been taken into consideration in [13]. Recently, a self-validated computing framework for indirect loadability analysis has been proposed in [14].

However, all above mentioned guidelines [11,12] do not account for the effect of rain precipitation, which can have a significant impact on the cooling of the line in rainy conditions. Recently, a DTR model with consideration of precipitation has been introduced in [15]. The presented model significantly improves the agreement between the computed and measured skin temperatures in rainy conditions in comparison with the CIGRE or IEEE std. 738-2012 models. This paper proposes improvements of the model in [15]. Namely, instead of steady-state heat balance, radial and temporal dependant heat transport is considered, evaporation due to drying is introduced in addition to evaporation due to the incoming rain flux, and dependence of the wetted area on the precipitation rate is incorporated to cover broader range of rain rates.

The rest of the paper is structured as follows. First, the mathematical model describing heat generation and heat transport within the overhead line, including heat exchange with the surrounding, is presented. The paper continues with description of an in-house experimental site used to perform reference measurements [16–18]. In the results section, a comparison of the model results with the measurements is presented. It is clearly demonstrated that the model shows good agreement with the measurements.

2. The DTR physical model

The numerical model for dynamic thermal rating presented in this paper is based on the CIGRE equilibrium model [11]; however, extended with additional terms describing the rain precipitation [15] and the radial diffusion of heat through the power line [19]. The problem is schematically presented in Fig. 1. A heat transfer within an aluminium conductor is solved as

$$\lambda_{Al} \frac{1}{r} \frac{\partial}{\partial r} r \frac{\partial}{\partial r} T_{Al} + q_i(T_{Al}) = \rho_{Al} c_{pAl} \frac{\partial T_{Al}}{\partial t}, \quad (1)$$

and within a steel core as

$$\lambda_{St} \frac{1}{r} \frac{\partial}{\partial r} r \frac{\partial}{\partial r} T_{St} = \rho_{St} c_{pSt} \frac{\partial T_{St}}{\partial t}. \quad (2)$$

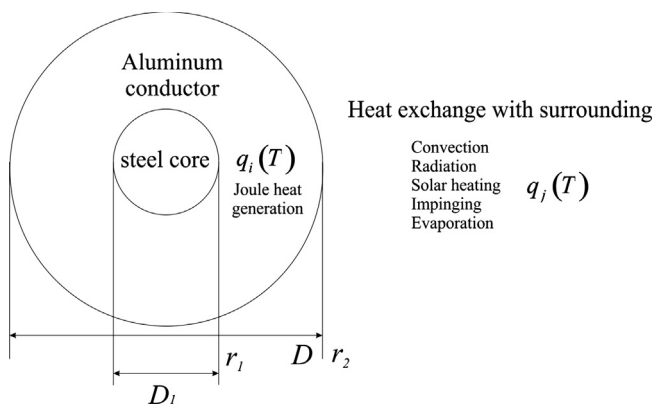


Fig. 1. Scheme of the DTR core problem.

The problem is closed with the following boundary conditions

$$\left. \frac{\partial T_{St}}{\partial r} \right|_{r=0} = 0, \quad (3)$$

$$\left. \frac{\partial T_{St}}{\partial r} \right|_{r=r_1} = \left. \frac{\partial T_{Al}}{\partial r} \right|_{r=r_1}, \quad (4)$$

$$T_{St}(r_1) = T_{Al}(r_1), \quad (5)$$

$$-\lambda_{Al} \left. \frac{\partial T}{\partial r} \right|_{r=r_2} = \sum_j q_j, \quad (6)$$

and the initial state

$$T(r, t = 0) = T_a, \quad (7)$$

where $\lambda_{(Al,St)}$, r , T , q_i , ρ and c_p stand for effective thermal conductivity [19], radii, temperature, heat source term, density and specific heat capacity, respectively, q_j describe different heat terms due to the weather conditions and T_a stands for ambient temperature. The index *st* stands for steel and *al* form aluminium. The radius $r_1 = D_1/2$ stands for interface between the steel core and the aluminium conductor and $r_2 = D_2/2$ for the skin of the power line. In Eq. (2), we assume that only small portion, i.e. below 1%, of electric current flows through the steel core [19].

The Joule heating is described as

$$q_j = \frac{4}{\pi D^2} I^2 R(T) \left[\frac{W}{m^3} \right] \quad (8)$$

with temperature dependant conductivity $R(T)$ defined as [11]

$$R(T) = R_{20} (1 + \alpha_{20} (T - 20 \text{ } ^\circ\text{C})), \quad (9)$$

where R_{20} stands for resistivity at 20 °C, $\alpha_{20} = 4.5e - 3 \text{ } ^\circ\text{C}^{-1}$ for the thermal resistance coefficient, and D stands for the line diameter.

The convection is incorporated as

$$q_c = -h(T_s - T_a) \left[\frac{W}{m^2} \right], \quad (10)$$

with h standing for the convection coefficient [11] that relates to the Nusselt number as $Nu = hD/\lambda_a$ and λ_a is the air thermal conductivity defined as

$$\lambda_a = 2.368 \cdot 10^{-2} + 7.23 \cdot 10^{-5} T_f - 2.763 \cdot 10^{-8} T_f^2 \left[\frac{W}{mK} \right], \quad (11)$$

with the film temperature $T_f = (T_a + T_s)/2$, where T_s is the surface temperature of the conductor. The Nusselt number is determined empirically with $Nu = BRE^n$ [20,21], where B and n stand for empirical parameters that characterize the power line properties – wind angle and natural convection, and Re stands for the Reynolds number $Re = uD/v_f$, with u standing for effective wind velocity, i.e. normal component of the wind regarding the power line, and v_f is the kinematic viscosity computed as:

$$v_f = \frac{1}{\rho_a} (17.239 + 4.635 \cdot 10^{-2} T_f - 2.03 \cdot 10^{-5} T_f^2) \cdot 10^{-6} \left[\frac{m^2}{s} \right], \quad (12)$$

$$\rho_a = \frac{1.293 - 1.525 \cdot 10^{-4} H + 6.379 \cdot 10^{-9} H^2}{1 + 0.00367 T_f} \left[\frac{kg}{m^3} \right], \quad (13)$$

where H stands for altitude of the power line.

The above model is only one among several empirical relations defining the heat transfer due to convection, e.g. the Churchill–Bernstein relation [22], the McAdams relation [23], the Zhukavskas relation [24], etc.

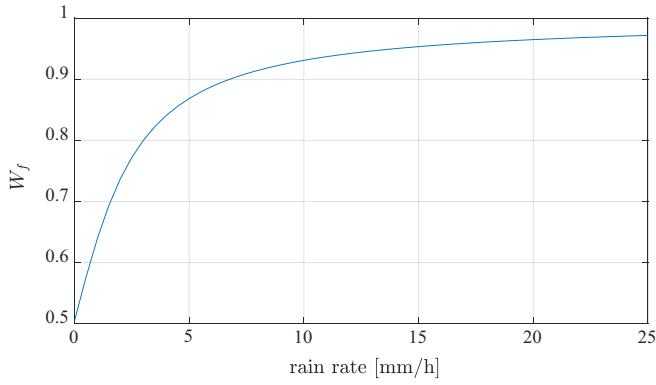


Fig. 2. Wetted factor dependency on the rain rate.

Table 1
Specifications of power lines.

	243-AL1/39-ST1A	490-AL1/64-ST1A
ρ_{St} [kg/m ³]	2703	2703
ρ_{Al} [kg/m ³]	7780	7780
c_{pAl} [J/kg K]	897	897
c_{pSt} [J/kg K]	481	481
λ_{AlSt} [W/mK]	1.1	0.67
R [Ω /m]	$1.3 \cdot 10^{-4}$	$5.7 \cdot 10^{-5}$
ε	0.6	0.6
B	0.27	0.45
n	0.68	0.56
α_s	0.5	0.5
r_1 [m]	0.0035	0.0045
r_2 [m]	0.0095	0.0133

The radiation term is introduced as

$$q_r = -\sigma_B \varepsilon_s (T_s^4 - T_a^4) \left[\frac{W}{m^2} \right], \quad (14)$$

where $\sigma_B = 5.67$ [W/m² K⁴] and ε_s stand for the Stefan-Boltzmann constant and emissivity, respectively. The solar heating is modelled as

$$q_s = \frac{\alpha_s I_T}{\pi} \left[\frac{W}{m^2} \right], \quad (15)$$

where I_T stands for measured solar intensity and α_s for absorptivity. The impinging of the rain is considered as [25]

$$q_{im} = -\frac{0.71}{\pi} c_w f_p (T_s - T_a) \left[\frac{W}{m^2} \right], \quad (16)$$

with $c_w = 4.2$ kJ/kg K standing for the specific heat of water, and the rain mass flux defined as [15,26]

$$f_p = \sqrt{\left(\frac{10^{-3}}{3600} P \rho_w \right)^2 + (u 6.71^{-5} P^{0.846})^2} \left[\frac{kg}{m^2 s} \right], \quad (17)$$

with P standing for the rain rate and $\rho_w = 1000$ [kg/m³] for water density. Finally, the evaporation is considered as

$$q_e = -W_f f_e L_e \left[\frac{W}{m^2} \right], \quad (18)$$

with evaporation mass flux f_e introduced as

$$q_e = \frac{hk(1-r)e_s}{c_p p} \left[\frac{kg}{m^2 s} \right], \quad (19)$$

where W_f stands for the wetted factor, $L_e = 2500$ kJ/kg stands for the evaporation latent heat, $c_p = 1$ kJ/kg K for the specific heat of the air, p for air pressure, $k = 0.62$ for the ratio of the molecular



Fig. 4. Digital temperature sensor on the surface of a conductor loop connected to a communication data bus.

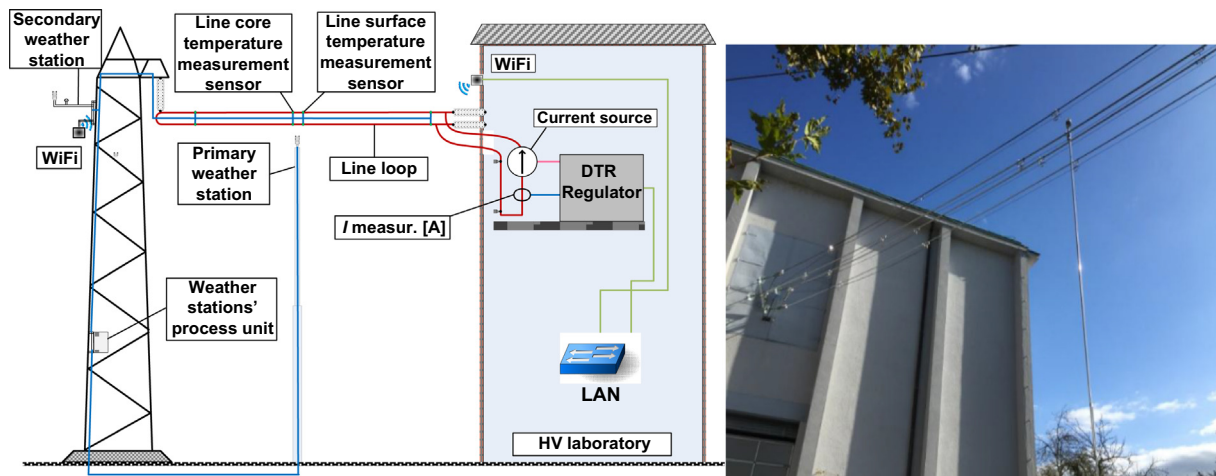


Fig. 3. Testing site for DTR uncertainty evaluation with two conductor current loops in X configuration.

weights of water vapour and dry air, and e_s for the saturation pressure, defined as

$$e_s(T) = e_{s0} e^{\left(\frac{L_v}{R_v} \left(\frac{1}{T_0} - \frac{1}{T} \right) \right)}, \quad (20)$$

with $e_{s0} = 6.1$ hPa and $R_v = 461$ J/kg K.

Although several authors assume constant wetted factor W_f , e.g., in $W_f = 0.5$ in [25,27], and [15] in $W_f = 1.0$, we propose that the wetted factor depends on the rain intensity $W_f(P)$ as:

$$W_f(P) = \frac{1.6 + \text{atan}(1600f_p)}{\pi/2 + 1.6}. \quad (21)$$

Only a half of the power line is wet [25,27] at low rain intensities; however, with increasing the precipitation rate, also the wetted area increases (Fig. 2).

Evaporation also does not stop when precipitation stops, as assumed in [15,25,27], but continues to cool the line as long as the line is wet. Although the drying of the line is a complex interplay of running-off water [28], corona effects [29,30] and evaporation, in this paper we assume simple mass continuity based model

$$\frac{dm_w}{dt} = f_e - f_p, \quad (22)$$

where m_w stands for the mass of water on the power line, with limitation that there cannot be more water on the line as dictated by (21), assuming additional relation $m_w = 2\pi r d_w W_f \rho_w$, where $d_w = 1$ mm stands for the average thickness of the water layer that corresponds to the measured average radius of droplets on the line during rain reported in [30].

The above model can be solved in a closed form for some limited scenarios [19]; however treating non-linear boundary conditions and time dependant simulation requires a numerical approach. In this paper, an implicit Finite Differences Method with 200 nodes and time step $\Delta t = 1$ s is used in all computations.

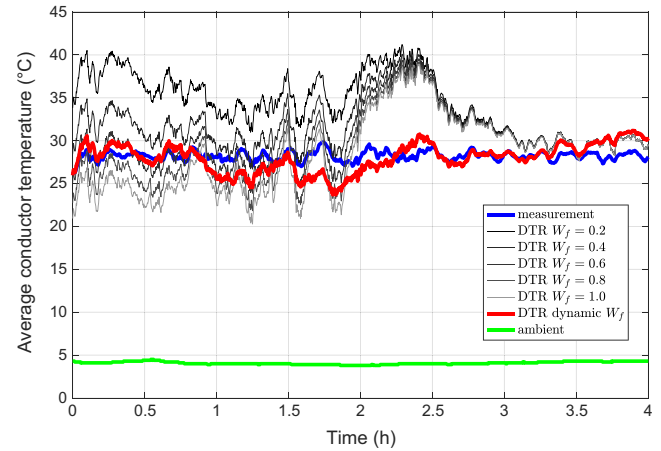


Fig. 6. Measured and calculated average conductor temperatures (results 1).

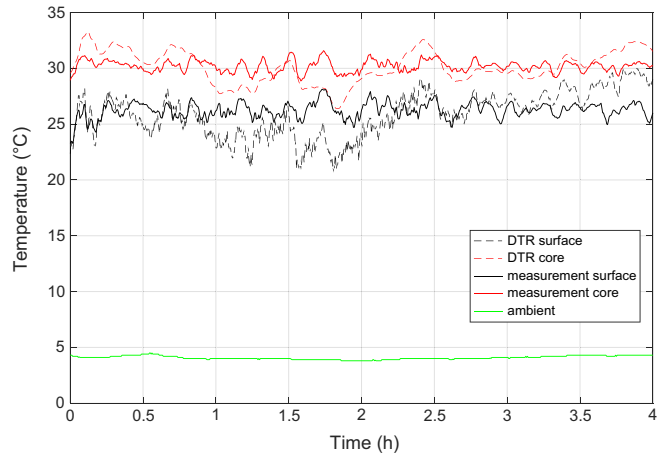


Fig. 7. Measured and calculated conductor temperatures (results 1).

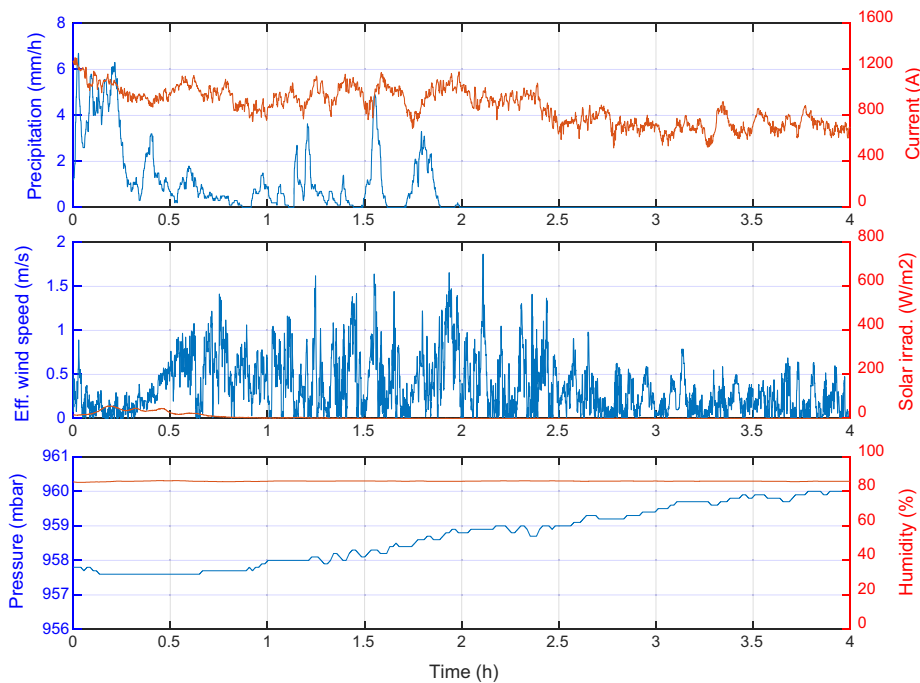


Fig. 5. Ambient weather conditions of measurement 1.

3. Experimental setup

The numerical model is validated by comparing the computed results under different weather conditions against measurements. The in-house testing site for the experimental measurements [16–18] supports various types of power conductors; however, the standard power conductors 243-AL1/39-ST1A and 490-AL1/64-ST1A (Table 1) have been tested in the form of current loops. The schematic representation of the testing site is shown in Fig. 3.

The selected conductor loop is powered with AC current through a laboratory class 0.1% precision current transformer with 2500 A:5 A ratio. The length of the loop is 47 m. In addition, the DTR regulator can be used to maintain the conductor on a specified temperature. The regulator is responsive enough to compensate sudden changes in ambient conditions, e.g. gusts of wind. A hybrid DTR current regulator is employed. PID regulation was expanded with an adaptive fuzzy control to meet the requested temperature tolerances within ± 2.5 °C. The power source is a 350 kV A transformer that feeds the precision current transformer.

Each conductor loop is equipped with 8 digital temperature sensors, namely, 2 inside the conductor core and 6 on the surface (Fig. 4). The primary temperature sensors used for the regulation are placed close to the weather station to ensure consistent measurements from common points. All sensors are calibrated within ± 0.5 °C accuracy in the range of -40 °C to 125 °C.

The weather data is collected within 20 cm off the conductor loops to capture weather data as precisely as possible, using ultrasonic wind speed and direction measurements. Besides information about wind, the weather station also measures solar irradiation (W/m^2), ambient temperature (°C), pressure (bar), relative humidity (%) and rain intensity (mm/h).

4. Results

In this section, the results of measured and calculated conductor temperatures are presented. In total, 16 h of measurements performed on four rainy days are taken into consideration. In measurement 3, the conductor 243-AL1/39-ST1A was used, while in

the other three measurements, the conductor 490-AL1/64-ST1A was used.

4.1. Measurement 1

Fig. 5 shows the first set of ambient and current measurements, i.e. the inputs for the model, for the 4 h interval. The regulator on the test polygon was set to maintain conductor temperature at approximately 30 °C.

Rainfall of varying intensity lasted for approximately 2 h. The effective wind velocity was below 2 m/s and the solar irradiation was minimal. The pressure and humidity were relatively constant at 960 mbar and 85%, respectively.

Using the data presented in Fig. 5, the temperatures of the power line are computed with the DTR model presented in Section 2. In Fig. 6, the computed conductor temperatures are compared with the measurements. The temperatures are presented in terms of averaged skin and core temperatures.

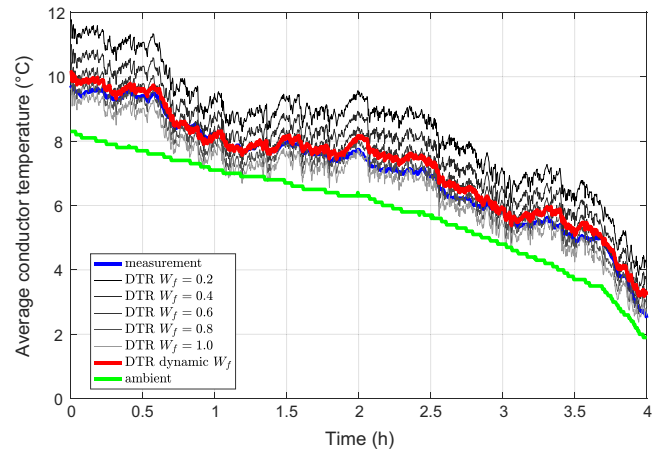


Fig. 9. Measured and calculated conductor temperatures (results 2).

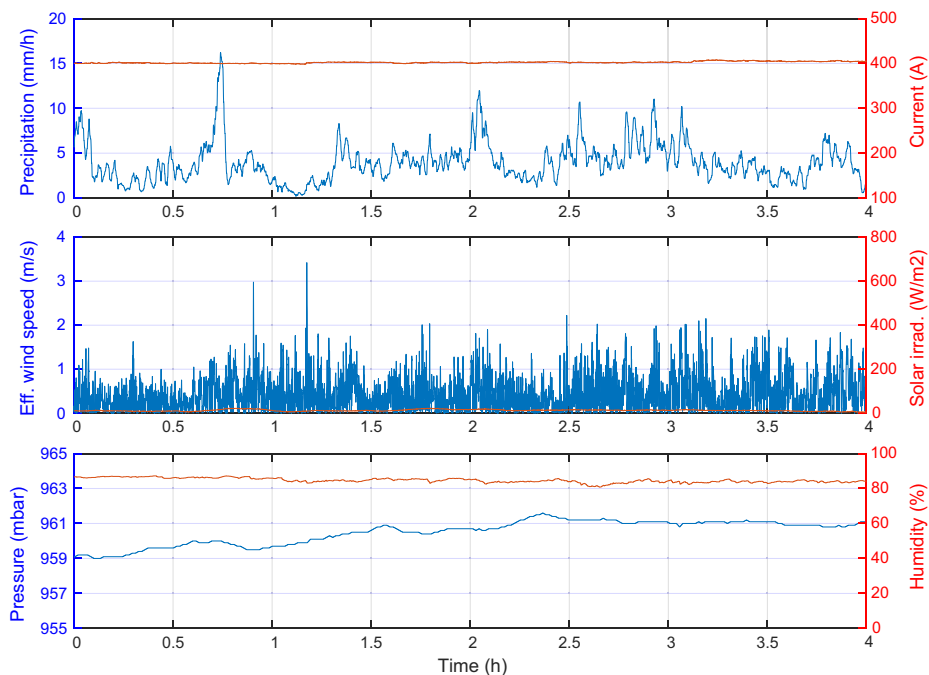


Fig. 8. Ambient weather conditions of measurement 2.

To demonstrate the effect of different wetted factor models on the results, comparison of results for different constant W_f and dynamic wetted factor (21) is performed. The results for the case with a constant $W_f = 0.2$ are denoted with a black line, while different gray line tones depict 4 more results, ranging from $W_f = 0.4$ –1.0. The thick red line shows average conductor temperature for dynamic W_f obtained according to (21). The measured average conductor temperature is shown with a thick blue line and the ambient temperature with a green line. The temperatures calculated with constant W_f have a noticeable discrepancy from the measurements for the period of 2–3 h. The rainfall subsides after 2 h, however, the conductor is still wet and cools down due to evaporation. The DTR algorithm with constant W_f does not take this into account and consequently the obtained temperature is greater than the actual one. On the other hand, dynamic W_f does consider this effect, and for this case the calculated and measured temperatures are in good agreement. Also during the periods with rainfall, the dynamic wetted factor model gives much better results in comparisons with a constant wetted factor model.

In Fig. 7, the measurements of conductor surface and core temperatures, along with the calculated results using dynamic W_f , are presented.

4.2. Measurement 2

The next set of measurements is shown in Fig. 8. During the 4-h period, the current was constant at 400 A, while the precipitation was mostly below 10 mm/h. The wind speed rarely exceeded 2 m/s and the solar irradiation was negligible. Both the pressure and humidity were again relatively constant at 960 mbar and 85%, respectively.

The comparison of an average conductor temperature results for different constant W_f and dynamic wetted factors is shown in Fig. 9.

4.3. Measurement 3

The third set of measurements is shown in Fig. 10. The set-point of the conductor current was changed 3 times in a 2-h period. The

rainfall was below 6 mm/h, while the effective wind speed was approximately 1.5 m/s. The solar irradiation was again small. The pressure was 980 mbar and the humidity ranged from 80% to 85%.

The DTR calculation and measurements of the average conductor temperatures are shown in Fig. 11. As in the previous two cases, the DTR temperature calculation using dynamic W_f overall agrees the best with the measurements.

4.4. Measurement 4

The last 6-h set of measurements are shown in Fig. 12. The rain intensity was smaller and did not exceed 2 mm/h. The conductor current was regulated to maintain conductor temperature at approximately 20 °C. The wind speed was relatively low and mostly below 2 m/s. The solar irradiation was below 200 W/m². The pressure was 970 mbar and the humidity was 85%.

The use of constant wetted factor $W_f = 0.8$ in Fig. 13 shows a relatively good agreement of the calculated conductor temperature with the measured one, but only in certain intervals with rainfall.

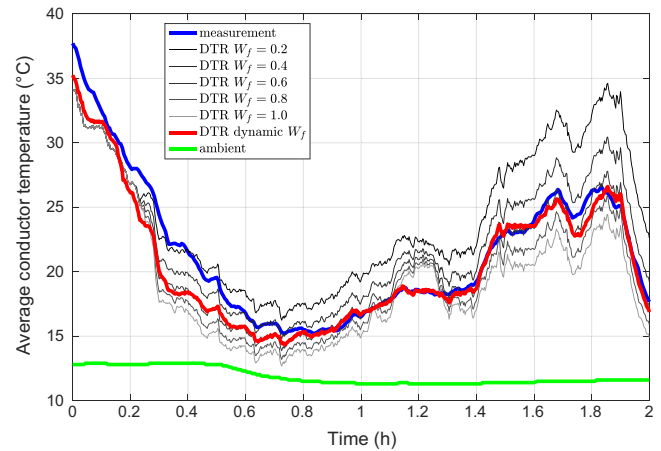


Fig. 11. Measured and calculated conductor temperatures (results 3).

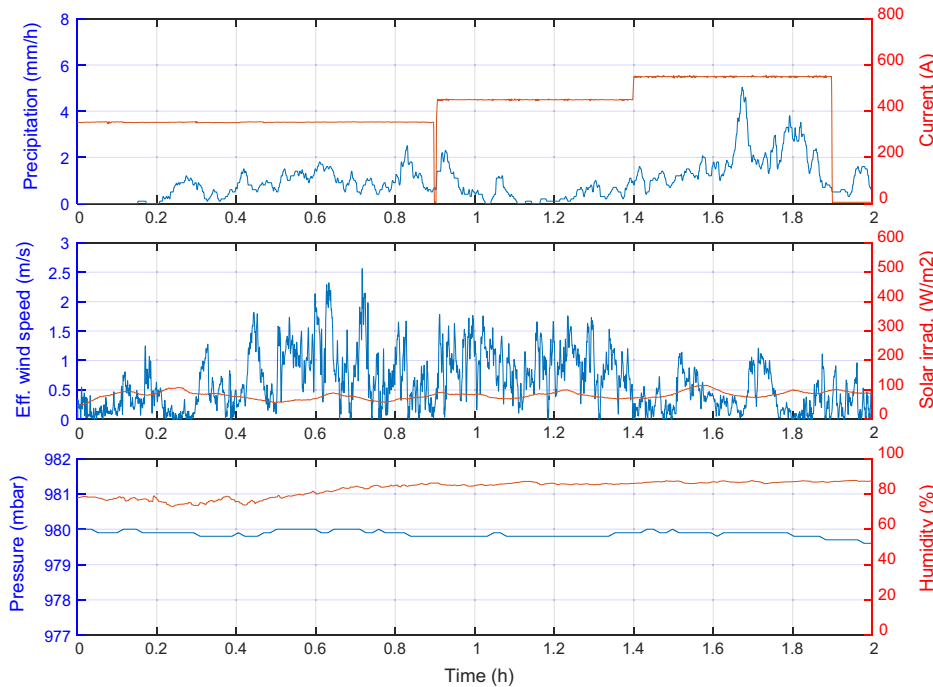


Fig. 10. Ambient weather conditions of measurement 3.

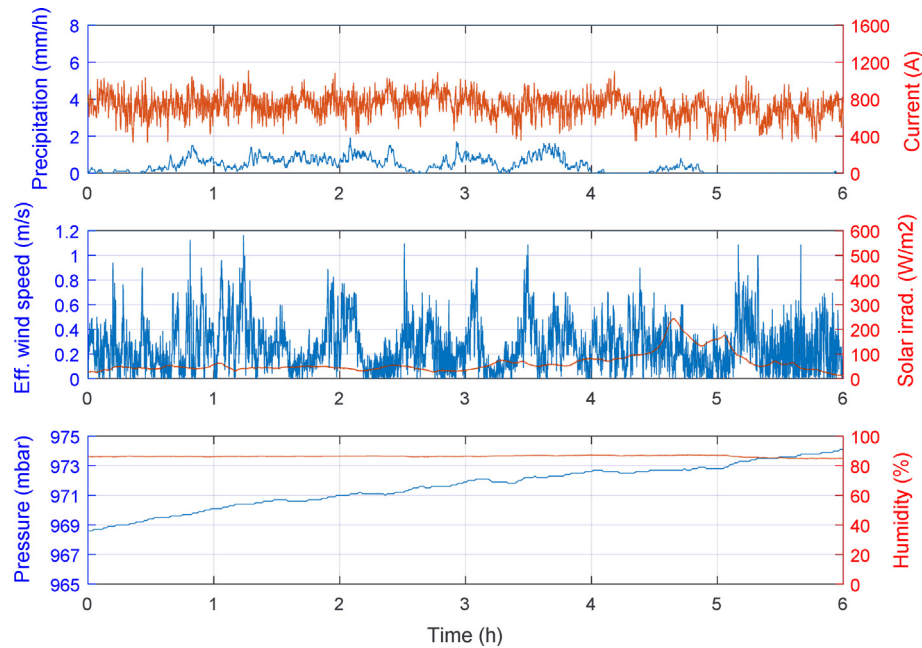


Fig. 12. Ambient weather conditions of measurement 4.

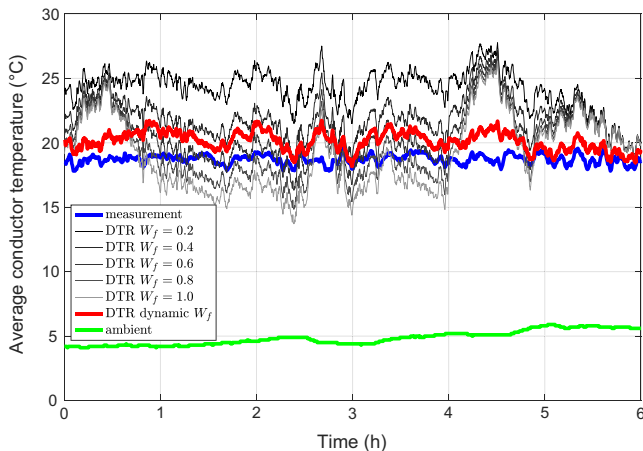


Fig. 13. Measured and calculated conductor temperatures (results 4).

On the other hand, the conductor temperature calculated with dynamic wetted factor has a practically constant deviation from the measurements in the range below 5 °C.

5. Conclusions

In this paper, an improved numerical model for Dynamic Thermal Rating (DTR) of overhead power lines, with emphasis on the consideration of the cooling of the line due to precipitation, is presented. The model considers Joule heating, heat transport through the power line, and heat exchange due to convection, radiation, evaporation, rain impinging and solar heating. The evaporation is additionally supported with wetted factor dependency on the precipitation rate and with a model that includes also the drying of the line. The model also considers radial temperature dependency.

The presented DTR model is validated through comparison of numerically computed temperatures of the power line with the measurements provided by an in-house testing site. It is demonstrated, in addition to the well-accepted model terms, that a simple

dynamic wetted factor model gravely improves the results, especially with unstable precipitation. Although using static wetted factor might work well for some cases, in general for all cases, dynamic factor results in a much better agreement with the measured data. The inclusion of the drying effect also improves the model response in transitions after the end of precipitation. This phenomenon can be neglected in a steady rainy weather; however, it plays an important role in unstable weather conditions when the overhead line might be in a drying regime considerable part of the time.

In future work, we will focus on the modelling the flow structures near the conductor to directly model the heat exchange due to convection, which has the greatest impact on the results. We expect to improve the response and generality of the model. With the existent model, we need to determine the parameters B and n for each conductor through measurements; however, with a full model that would not be necessary anymore.

From experimental point of view, we plan to perform more measurements, especially on warmer days, to assess the behaviour of the dynamic wetted factor in high temperature regimes that are more interesting for TSOs. We will also validate the model further by new measurements at different rain rates and effective wind velocities.

Acknowledgment

The authors acknowledge the financial support from the Slovenian Research Agency (research core funding No. P2-0095). The authors also wish express gratitude to the Slovenian TSO ELES, d. o.o. for its support in funding the DTR testing site.

References

- [1] Berizzi A. The Italian 2003 blackout. In: IEEE power engineering society general meeting, vol. 2; 2004. p. 1673–9.
- [2] Jadhav HT, Bamane PD. Temperature dependent optimal power flow using g-best guided artificial bee colony algorithm. Int J Electr Power Energy Syst 2016;77:77–90. <http://dx.doi.org/10.1016/j.ijepes.2015.11.026>.
- [3] Cimini CA, Fonseca BQA. Temperature profile of progressive damaged overhead electrical conductors. Int J Electr Power Energy Syst 2013;49:280–6. <http://dx.doi.org/10.1016/j.ijepes.2012.12.015>.

- [4] EN 50182:2002. Conductors for overhead lines. Round wire concentric lay stranded conductors; 2002.
- [5] Gubelj N, Banič B, Lovrenčič V, Kovač M, Nikolovski S. Preventing transmission Line damage caused by ice with smart on-line conductor monitoring. *IEEE*; 2016. p. 155–63.
- [6] Yan D, Liao Y. Online estimation of power transmission line parameters, temperature and sag. In: 2011 North American power symposium. p. 1–6.
- [7] Oleinikova I, Mutule A, Putnins M. PMU measurements application for transmission line temperature and sag estimation algorithm development. *IEEE*; 2014. p. 181–5.
- [8] Ritzmann D, Wright PS, Holderbaum W, Potter B. A method for accurate transmission line impedance parameter estimation. *IEEE Trans Instrum Meas* 2016;65:2204–13.
- [9] Shi D, Tylavsky DJ, Koellner KM, Logic N, Wheeler DE. Transmission line parameter identification using PMU measurements. *Eur Trans Electr Power* 2011;21:1574–88. <http://dx.doi.org/10.1002/etep.522>.
- [10] Howington BS, Ramon GJ. Dynamic thermal line rating summary and status of the state-of-the-art technology. *IEEE Trans Power Deliv* 1987;2:851–8.
- [11] Guide for thermal rating calculations of overhead lines. CIGRE; 2014.
- [12] IEEE standard for calculating the current-temperature relationship of bare overhead conductors. *IEEE Std. 738–2012*; 2014.
- [13] Piccolo A, Vaccaro A, Villacci D. Thermal rating assessment of overhead lines by Affine Arithmetic. *Electr Power Syst Res* 2004;71:275–83. <http://dx.doi.org/10.1016/j.epsr.2004.01.018>.
- [14] Carlini EM, Pisani C, Vaccaro A, Villacci D. A reliable computing framework for dynamic line rating of overhead lines. *Electr Power Syst Res* 2016;132:1–8. <http://dx.doi.org/10.1016/j.epsr.2015.11.004>.
- [15] Pytlak P, Musilek P, Lozowski E, Toth J. Modelling precipitation cooling of overhead conductors. *Electr Power Syst Res* 2011;81:2147–54.
- [16] Djurica V, Lakota G, Maksič M, Kosmač J, Kostevc J. A reference testing site for evaluation of dynamic thermal rating algorithm uncertainties in the operation of transmission power lines. In: The 19th international symposium on high voltage engineering. Paper 2015.
- [17] Djurica V, Lakota G, Maksič M, Kosmač J, Kostevc J, Jevnikar K. Preskusni poligon za oceno negotovosti DTR algoritmov = Methodology for comparing exposure of electric distribution grid to lightning. In: Dvanajsta konferenca slovenskih elektroenergetikov. Paper 2015.
- [18] Souvent A, Djurica V, Jevnikar K. Determination of uncertainty limits of DTR algorithms used in sumo system. Ljubljana, Slovenija: Elektrotehniški inštitut Milan Vidmar; 2015.
- [19] Morgan VT. The radial temperature distribution and effective radial thermal conductivity in bare solid and stranded conductors. *IEEE Trans Power Deliv* 1990;5:1443–52.
- [20] Iglesias J, Watt G, Douglass D, Morgan V, Stephen R, Bertinat M, et al. Guide for thermal rating calculations of overhead lines. In: CIGRE, editor; 2014.
- [21] Morgan VT. The heat transfer from bare stranded conductors by natural and forced convection in air. *Int J Heat Mass Transfer* 1973;16(11):2023–34.
- [22] Churchill SW, Bernstein M. A correlating equation for forced convection from gases and liquids to a circular cylinder in crossflow. *J Heat Transfer* 1977;99(2):300–6.
- [23] McAdams WH. Heat transmission. New York: McGraw-Hill Book Company Inc.; 1959.
- [24] Zhukauskas A, Žiugžda J. Heat transfer of a cylinder in crossflow. Hemisphere Pub; 1985.
- [25] Zsolt P, Masoud F, Lszl KI. Assessment of the current intensity for preventing ice accretion on overhead conductors. *IEEE Trans Power Deliv* 2007;22:565–74. <http://dx.doi.org/10.1109/TPWRD.2006.877091>.
- [26] Jones KF. Ice accretion in freezing rain. DTIC Document; 1996.
- [27] Systems for prediction and monitoring of ice shedding, anti-icing and de-icing for overhead power line conductors and ground wires. Paris: CIGRE; 2010.
- [28] Weidner DE, Schwartz LW, Eres MH. Simulation of coating layer evolution and drop formation on horizontal cylinders. *J Colloid Interface Sci* 1997;187:243–58.
- [29] Pfeiffer M, Schultz T, Hedtke S, Franck CM. Explaining the impact of conductor surface type on wet weather HVDC corona characteristics. *J Electrostat* 2016;79:45–55. <http://dx.doi.org/10.1016/j.elstat.2015.12.003>.
- [30] Schultz T, Pfeiffer M, Franck CM. Optical investigation methods for determining the impact of rain drops on HVDC corona. *J Electrostat* 2015;77:13–20. <http://dx.doi.org/10.1016/j.elstat.2015.06.007>.